Ubiquitous Membrane-bound DNase Activity in Podosomes and Invadopodia

Kaushik Pal[1], Yuanchang Zhao[1], Yongliang Wang[1], Xuefeng Wang[1,2*]

[1]Department of Physics and Astronomy, Iowa State University, Ames, IA 50011, USA

[2]Molecular, Cellular, and Developmental Biology interdepartmental program, Ames, IA 50011, USA

*To whom correspondence may be addressed. Email: xuefeng@iastate.edu

Abstract:

Podosomes and invadopodia, collectively termed invadosomes, are adhesive and degradative membrane structures formed in many types of cells, and well known for recruiting various proteases. However, another major class of degradative enzymes, deoxyribonuclease (DNase), remains unconfirmed and not studied in invadosomes. Here, using surface nuclease sensor (SNS), we unambiguously demonstrated that invadosomes recruit DNase to their core regions which degrade extracellular double-stranded DNA. We further identified the DNase as GPI-anchored membrane-bound DNase X. DNase recruitment is ubiquitous and consistent in invadosomes of all tested cell types. DNase activity exhibits within a minute after actin nucleation, functioning concomitantly with protease in podosomes but preceding it in invadopodia. We further showed that macrophages form DNase-active podosome rosettes surrounding bacteria or micro-patterned antigen islets, and the podosomes directly degrade bacterial DNA on a surface, exhibiting an apparent immunological function. Overall, this work reported DNase in invadosomes for the first time, suggesting a richer arsenal of degradative enzymes in invadosomes than known before.

Summary:

Pal et al. discovered that podosomes and invadopodia ubiquitously recruit membrane-bound DNase X which readily degrades extracellular double-stranded DNA. The authors also showed that macrophages, in response to immunogenic materials, form podosomes that degrade bacterial DNA on surfaces.

Introduction

Podosomes and invadopodia are micron-sized membrane protrusive structures that have both adhesive and degradative functions by interacting with the surrounding extracellular matrix (ECM) (Chen et al., 1985; Dalaka et al., 2020; Tarone et al., 1985). They are found in a wide range of cell types, with podosomes formed in monocytes, osteoclasts, dendritic cells, smooth muscle cells, *etc*., and invadopodia formed in many carcinoma cells. Although podosomes and invadopodia are found in different cell types, and their temporal dynamics are quite different, they share a significant structural and enzymatic similarities (Albiges-Rizo et al., 2009). Both structures have actin cores surrounded by peripheral adhesion rings consisting of integrin, vinculin, paxillin, etc. (Badowski et al., 2008; Branch et al., 2012). In recent literature, these two structures were often collectively termed invadosomes (Linder et al., 2011; Saltel et al., 2011). As formed in various cell types, invadosomes are highly versatile and involved in many physiological processes such as cell motility, cancer invasion and metastasis, matrix remodeling, bone structure maintenance, *etc.* (Eddy et al., 2017; Poulter et al., 2015; Raynaud-Messina et al., 2018; Ridley, 2011).

One characteristic feature of invadosomes is their enzymatically degradative function. Matrix degradation by invadopodia has been correlated with cancer metastasis and invasion (Desai et al., 2008; Poincloux et al., 2009). In parallel, the degradative nature of podosomes has been considered as an important factor regulating the migration and tissue infiltration of macrophages (Cougoule et al., 2010; Linder et al., 1999; Van Goethem et al., 2011), the phagocytes specialized in removing cellular debris and pathogens. Due to the physiological and pathological importance of their enzymatic functions, invadosomes have been pursued as pharmaceutical targets (Winer et al., 2018). Currently, the degradative ability of invadosomes is solely attributed to proteases such as serine proteases, ADAM proteases, and metalloproteases (Jacob and Prekeris, 2015; Lochter et al., 1998; Paz et al., 2014; Wagenaar-Miller et al., 2004). Surprisingly, DNase, another major class of enzymes found in the living system, has not been studied, identified, or even noticed in invadosomes.

In this work, we revealed that DNase is consistently and ubiquitously recruited to both podosomes and invadopodia. A surface-immobilized nuclease sensor (SNS) (Wang et al., 2019), which detects and images DNase activity at the cell-substrate interface by fluorescence, was applied to study podosomes (in human, mouse macrophage-like cells and fish macrophages) and invadopodia (in human and mouse cancer cell lines). Results showed strong local DNase activity in both podosomes and invadopodia. Co-imaging of structures and enzymatic activities in invadosomes confirmed that DNase is recruited quickly after the actin core nucleation in invadosomes and remains locally active at the core region. We further identified the DNase in invadosomes as DNase

X (Shiokawa et al., 2007), a glycosylphosphatidylinositol (GPI)-anchored membrane protein. We then devised a co-degradation assay, by which we revealed that DNase and proteases are active concomitantly in podosomes, whereas DNase activity preceded protease activity in invadopodia. These results suggest that podosomes are equipped with more degradative enzymes than known so far. To our knowledge, this is the first report of DNase activity at the cell-substrate interface in invadosomes.

We then investigated the physiological function of DNase activity in podosomes in macrophages. On both *E. coli*-immobilized surfaces and antigen micro-patterned surfaces, macrophages patrolled on the surface by forming DNase-active podosomes in the cell front, and quickly reacted to immunogenic targets by forming podosome rosettes around *E. coli* or antigen islets. We further showed that podosomes in macrophages directly degrade bacterial DNA on the surface, demonstrating that macrophages can utilize podosomes to clean up extracellular pathogenic DNA without the need of internalizing it. We believe that this finding will be an important starting point to investigate more physiological functions of DNase in invadosomes.

Results

SNS reports DNase activity in invadosomes

Previous studies have discovered a plethora of adhesive, structural, and enzymatic proteins in invadosomes (Fig. 1a) (Buccione et al., 2004; Murphy and Courtneidge, 2011). Many proteases are known to take active roles in the function of invadosomes. DNase, as another major class of degradative enzymes, somehow remains unnoticed and uninvestigated in invadosomes. Here we applied two DNase sensors and total internal reflection fluorescence (TIRF) microscopy to investigate the DNase activity in invadosomes at the cell-substrate interface. The first DNase sensor is surface-immobilized Cy3-labeled double-stranded DNA (dsDNA), as shown in Fig. 1b. This sensor loses the dye if degraded by DNase and therefore reports DNase activity by fluorescence loss, resembling the classic dye-labeled gelatin degradation assay used to report protease activity of invadopodia (Berdeaux et al., 2004; Mueller et al., 1992). The other sensor is SNS (Fig. 1c), a dsDNA labeled by a quencher-dye pair at the opposite strands, and a biotin tag for surface immobilization through biotin-neutravidin interaction. Initially dark SNS becomes fluorescent if the dsDNA is degraded and dye is freed from the quencher, hence reporting DNase activity at the cell-substrate interface by fluorescence gain. Human macrophage-like THP-1 cells (activated with TGF-β1 (Rafiq et al., 2019) and called just THP-1 onwards) were plated on glass surfaces coated with these two types of sensors, respectively. On the surface coated with dye-labeled dsDNA, strong fluorescence loss in a punctate pattern was observed, co-localizing with podosomes that were identified by the actin cores and vinculin rings (Figs. 1d and 1f). To rule out the possibility that these dark puncta were caused by local dye bleaching or sensor detachment, THP-1 cells were plated on an SNS-coated surface where podosomes produced bright fluorescence puncta, confirming that the dsDNA construct in the SNS was degraded (Figs. 1e and 1g). These two assays confirmed that podosomes in THP-1 cells exhibit strong DNase activity in the core regions. Further verification was conducted to confirm that the DNase in the podosomes is dsDNA-

specific (fig. S1). Results showed that the DNase in podosomes degraded dsDNA regardless of DNA sequences, but did not degrade single-stranded DNA (ssDNA) or DNA/PNA (peptide nucleic acid) hybrid duplex which is supposed to be DNase-resistant. As the SNS specifically responds to DNase activity, ruling out potential false positive signal caused by dye bleaching, we adopted the SNS platform for all following experiments.

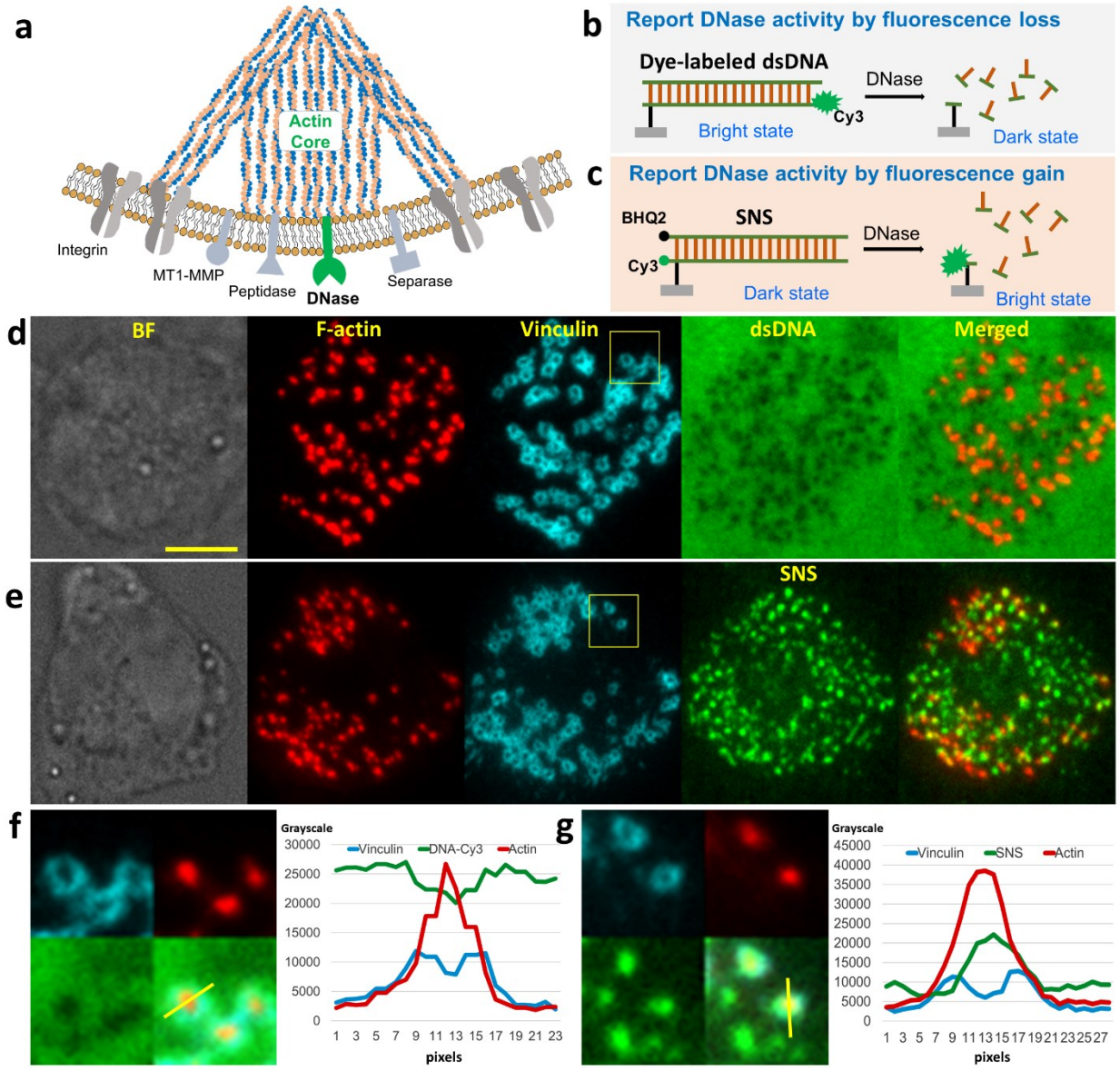

Fig. 1. DNase activity in invadosomes reported by surface nuclease sensor (SNS). (**a**) Basic invadosome structure and representative proteins. DNase depicted in green is revealed in this study. (**b**) Surface-immobilized Cy3-labeled dsDNA visualizes DNase activity by fluorescence loss. (**c**) SNS with a quencher-dye pair reports DNase activity by fluorescence gain. (**d**) A THP-1 cell on a surface coated with Cy3-labeled dsDNA. Podosomes were identified by the characteristic actin core and vinculin ring. dsDNA was degraded in a dark punctate pattern co-localized with the podosomes. (**e**) A THP-1 cell on an SNS immobilized surface, which showed DNA degradation in a bright punctate pattern co-localized with podosomes. Statistics show that 86±5% actin puncta are co-localized with SNS punctate

signal (600 podosomes over 20 cells). (**f**) and (**g**) are representative regions marked by yellow boxes in (d) and (e), respectively. Line profiles (marked by yellow lines) of Vinculin, F-actin and DNase sensor signal in single podosomes are also presented in (f) and (g). Scale bar: 5 μm.

We evaluated the consistency of DNase activity in podosomes. Co-imaging of F-actin and DNase activity of THP-1 cells showed that 86±5 % actin puncta are co-localized with SNS punctate signal (analyzed on the basis of 600 podosomes over 20 cells). The experiment was conducted more than three times, and the percentage did not vary significantly. Note that the actual percentage of invadosomes exhibiting DNase activity should be even higher than observed because DNase activity starts to appear ~1 minute later after the actin core nucleation (shown in the section of Temporal dynamics of DNase activity in podosomes) and therefore a small set of actin puncta have yet to produce any SNS signal. In the images, many SNS puncta have no corresponding actin cores. This is because invadosomes are subject to disassembly, while SNS surface records all historic DNase activity. As a result, there is a subset of SNS puncta where invadosomes have already disassembled.

DNase is ubiquitously recruited to invadosomes

To test if DNase is commonly recruited to invadosomes in different cell types, we have applied SNS assay to five cell types from different species, which form either podosomes or invadopodia: human macrophage-like THP-1, mouse macrophage-like RAW264.7, fish macrophages (identified in fig. S2), MDA-MB-231 human breast cancer cells, and MTC (mouse musculus thyroid carcinoma) cells. Podosomes in RAW264.7, THP-1 cells and fish macrophages were identified with imaging of actin cores. The latter two types of cells form invadopodia, which were identified with co-imaging of actin, cortactin and TKS5 (fig. S3-S4). All the five invadosome-forming cell lines exhibited significant DNase activity localized with the actin cores of invadosomes (Fig. 2a-e), suggesting that DNase recruitment by invadosomes is highly consistent and ubiquitous in the different cell types and species. SNS assay was also applied to CHO-K1 cells as a negative control (Uekita et al., 2001), which do not form podosomes or invadopodia. As expected, CHO-K1 cells did not form F-actin in a punctate pattern and exhibited no DNase activity on the SNS surface (Fig. 2f). A statistical analysis shows that over 80% of podosomes in RAW264.7, THP-1 and fish macrophages have exhibited DNase activities. Percentage of actin cores colocalizing with DNase activities in invadopodia are 80% in MDA-MB-231 and 46% in MTC, respectively (Fig. 2g).

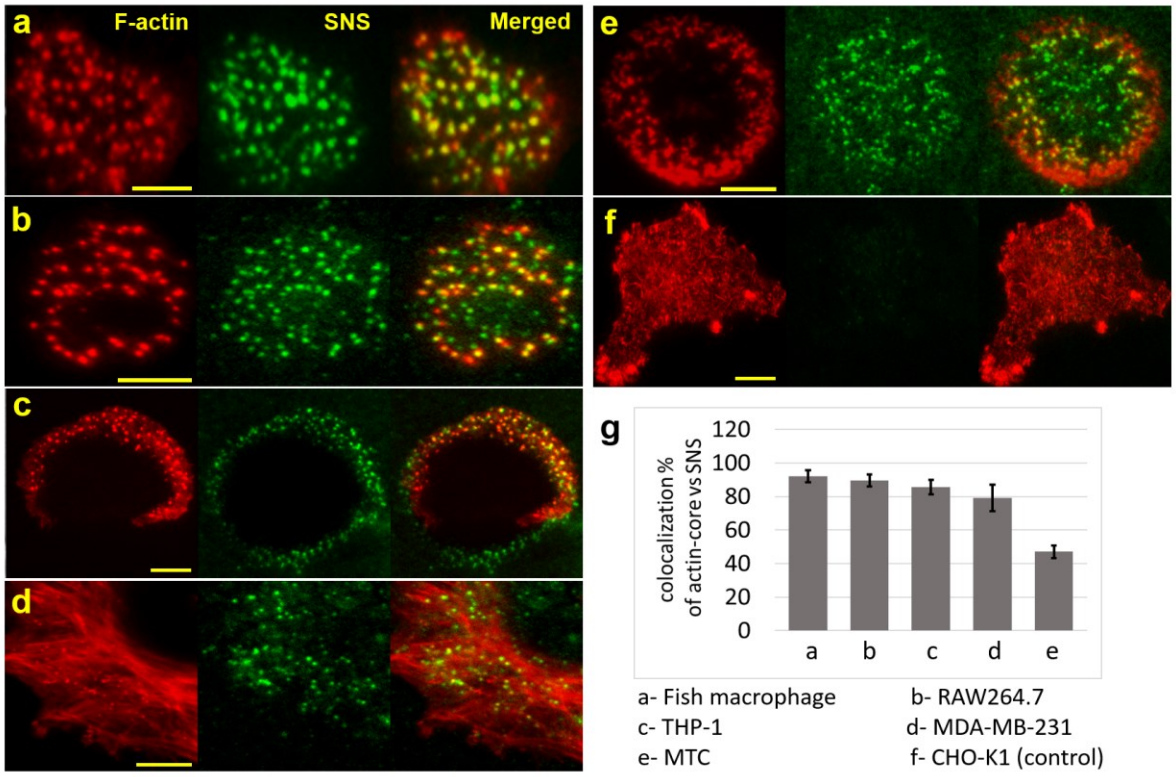

Fig. 2. Ubiquitous DNase activity in invadosome-forming cells. (**a-e**) RAW264.7, THP-1, fish macrophages, MDA-MB-231 and MTC, with former three forming podosomes and latter two forming invadopodia, exhibited DNase activity in punctate patterns. Scale bar: 5 µm. (**f**) CHO-K1 cell as a control does not form invadosomes (no actin core), and no DNase activity was observed at the cell-substrate interface. (**g**) Percentage of actin cores that are co-localized with strong SNS punctate signal (20 cells and 400-700 invadosomes are analyzed for each cell type). Error bars represent standard errors.

Temporal dynamics of DNase activity in podosomes

Podosomes and invadopodia have different temporal dynamics in terms of structures and functions. To investigate the temporal dynamics of the DNase activity relative to the structural formation of podosomes, we tested RAW264.7 cells stably transfected with lifeAct-GFP that reports F-actin on an SNS surface (Fig. 3a, Video 1). Fluorescence time-lapse imaging was performed to monitor both the SNS signal and actin nucleation in live cells. Note that the emerging time of SNS signal is not the time of DNase recruitment which may proceed DNase activity reported by the SNS signal. Nonetheless, the result revealed that the DNase activity in podosomes manifested quickly (within ~1 minute) after the initiation of actin nucleation and remains active (Figs. 3b and 3c) afterward, demonstrating strong enzymatic activity degrading extracellular DNA by podosomes. Further experiments were performed to test the correlation between the actin nucleation and DNase recruitment. It was found that the actin core formation is required for DNase recruitment to podosomes, as inhibiting actin polymerization with cytochalasin D abolished DNase activity in the punctate pattern. In contrast, inhibiting myosin II (another important structural component) in podosomes with blebbistatin had an insignificant effect on DNase activity (fig. S5).

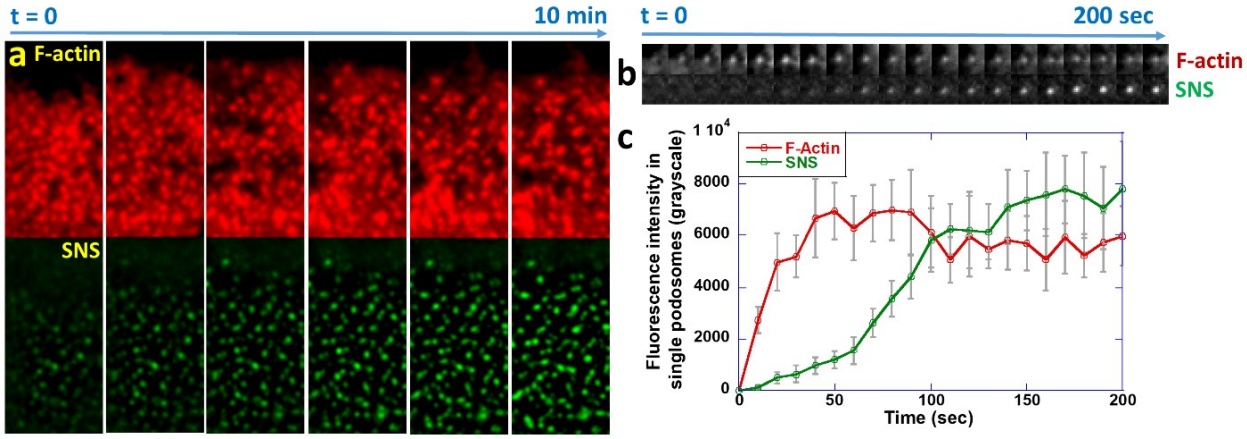

Fig. 3. Temporal dynamics of actin core nucleation and DNase activity. (**a**) F-actin and SNS signal reporting DNase activity was co-imaged in RAW264.7 transfected with lifeAct-GFP. (**b**) Time-series images of F-actin and SNS signal in one representative podosome (Video 1). (**c**) Temporal curves of F-actin and DNase activity averaged over 20 podosomes, showing that DNase activity manifests in about 1 minute after actin core nucleation.

DNase in invadosomes is GPI-anchored DNase X

The localized DNase activity in a punctate pattern suggests that the DNase in invadosomes is not secreted soluble protein, but likely membrane-bound. Otherwise, the SNS signal would not be narrowly localized in invadosomes because of the diffusion of soluble DNase. Because DNase X (also known as Deoxyribonuclease-1-like 1) was previously known as membrane-bound nuclease (Parrish et al., 1995), we hypothesized that the DNase in invadosomes is DNase X. Because DNase X is anchored on the cell membrane by glycophosphatidylinositol (GPI) (Paulick and Bertozzi, 2008) which is a common lipid anchor linking a protein to the cell membrane, we first tested whether the DNase in invadosomes is GPI-anchored. Treated with phosphatidylinositol-specific phospholipase C (PI-PLC), which cleaves the GPI anchor, DNase activity in podosomes in THP-1 cells was significantly reduced, and SNS signal was nearly zero under the treatment of 5 unit/mL PI-PLC (Figs. 4a and 4b). The unaltered actin core structures in PI-PLC treated cells suggests that the reagent does not prevent the structural formation of the podosomes. This result suggests that the DNase activity in podosomes is due to GPI-anchored nuclease which is likely DNase X. We further tested by immunostaining if the DNase in podosomes is DNase X. The immunostained spots of DNase X and the SNS puncta are well co-localized (Fig. 4c), suggesting that DNase X is recruited to podosomes. To further confirm the identity of the DNase, we knocked down DNase X expression in THP-1 cells with small interfering RNA (siRNA) targeting human DNase X mRNA. DNase X knockdown significantly reduced DNase X expression level in THP-1 cells (fig. S6). With DNase X knocked down, DNase activity in podosomes of THP-1 cells also significantly decreased (Figs. 4d and 4e), suggesting that DNase X is the major active DNase in podosomes. Collectively, we identified the DNase in podosomes as GPI-anchored DNase X.

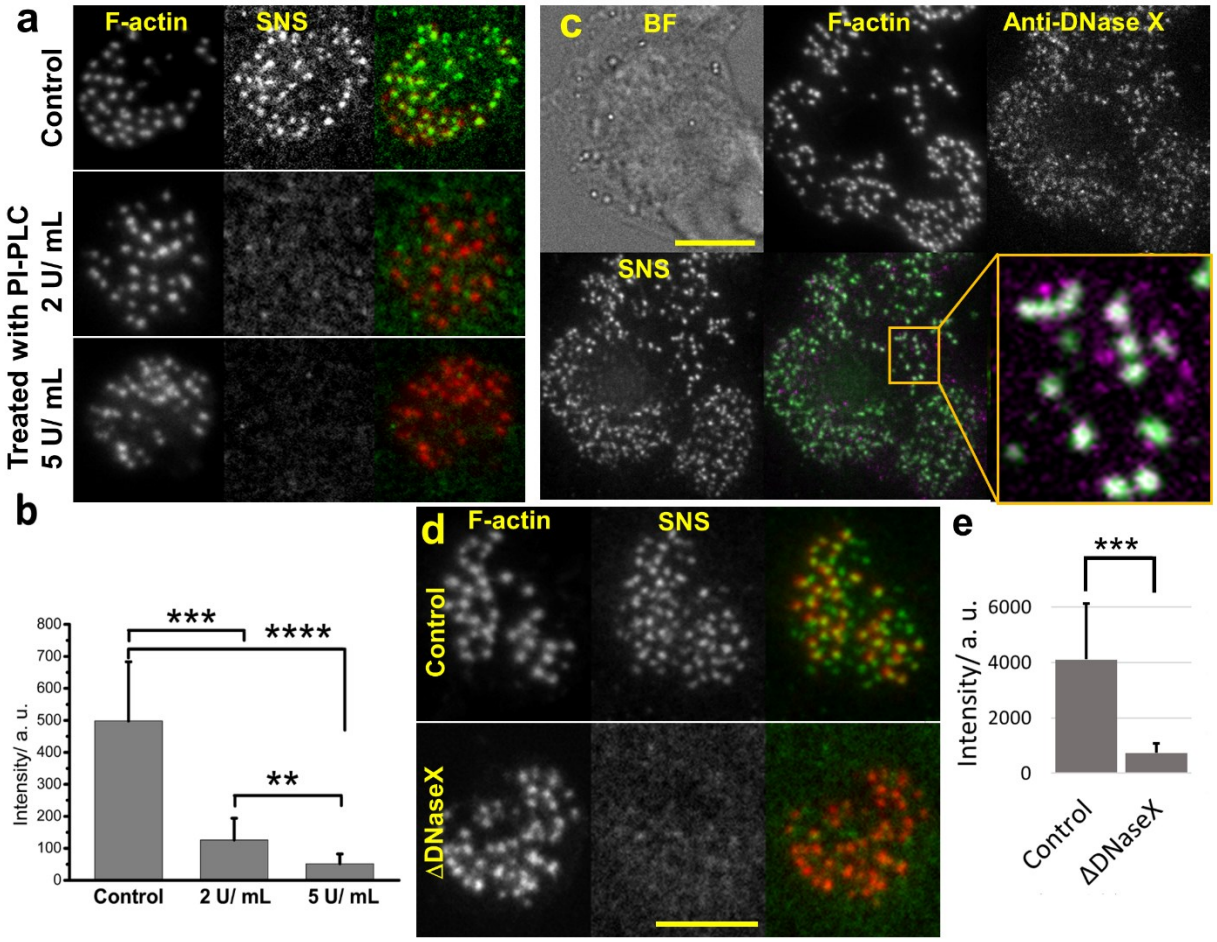

Fig. 4. Identification of the DNase in invadosomes. (**a**) SNS and F-actin signals in THP-1 cells treated with PI-PLC, which cleaves GPI anchors. (**b**) SNS signals in THP-1 cells with 20 cells for each data point, showing that PI-PLC significantly reduced the DNase activity in invadosomes. The merged figure consists of SNS signal in green and anti-DNase X signal in magenta. (**c**) Immunostaining of THP-l cells with anti-DNase X showed good colocalization between anti-DNase X and SNS signal. (**d**) THP-1 with DNase X gene knockdown (ΔDNase) and the control cell on the SNS surfaces. Podosomes formed normally in both sets of cells. (**e**) THP-1 with DNase X gene knockdown showed a significant reduction of DNase activity reported by SNS signal. The analysis was based on 20 cells for each data point. All significances were evaluated by two-tailed tests. Error bars represent standard deviations. Scale bar: 10 μm.

The capability of co-degrading DNA and matrix proteins by invadosomes

Enzymatic degradation is the crucial and prominent biochemical functionality of invadosomes. Previously, extensive research has been dedicated to investigating the degradation of ECM proteins by invadosomes (Berdeaux et al., 2004; Kelly et al., 1994). However, ECM also consists of extracellular DNA originating from apoptotic and necrotic cells, the NET (neutrophil extracellular traps) (Brinkmann et al., 2004), invading pathogens, *etc*. (Aucamp et al., 2018; Brinkmann et al., 2004). Here we designed a co-degradation assay to simultaneously monitor the degradation of both matrix protein and extracellular DNA by invadosomes. We coated glass surfaces with both SNS and dye-labeled (HyLight488) fibronectin (FN) and tested THP-1 and MTC cells on these surfaces. Time-lapse live-cell fluorescence imaging showed that podosomes

were formed in THP-1 cells and rapidly degraded both SNS (made of dsDNA) and FN nearly simultaneously (Figs. 5a, 5b and Video 2). This suggests that DNase may potentially participate in matrix degradation, with an enzymatic role parallel to that of proteases. In contrast, invadopodia formed in MTC cells exhibited rapid DNase activity, but no degradation of FN (due to protease activity) was observed within our time frame of imaging (1 h) (Fig. 5c, d, Video 3). Some previous studies showed that invadopodia exhibited detectable protease activity on the gelatin surface within 1 h (Artym et al., 2006). This discrepancy may be due to the fact that our assay was performed on the rigid glass surface, where invadopodia may have longer maturation time than those on the soft gel surface. Nonetheless, this experiment suggests that DNase activity manifests more rapidly than protease activity in invadopodia. To confirm that this effect is statistically significant, we repeated this test with imaging over a larger number of fixed cells on surfaces coated with SNS and FN. The result is consistent with the result of live-cell experiments. Podosomes in THP-1 cells degraded both dsDNA and FN, whereas invadopodia in MTC only degraded dsDNA (Figs. 5e and 5f). Overall, our results suggest that DNase activity is more ubiquitous and prompter than protease activity in invadosomes, potentially making it a superior biomarker for the identification of invadosomes, and also suggesting that DNase may play a prominent physiological role in invadosomes.

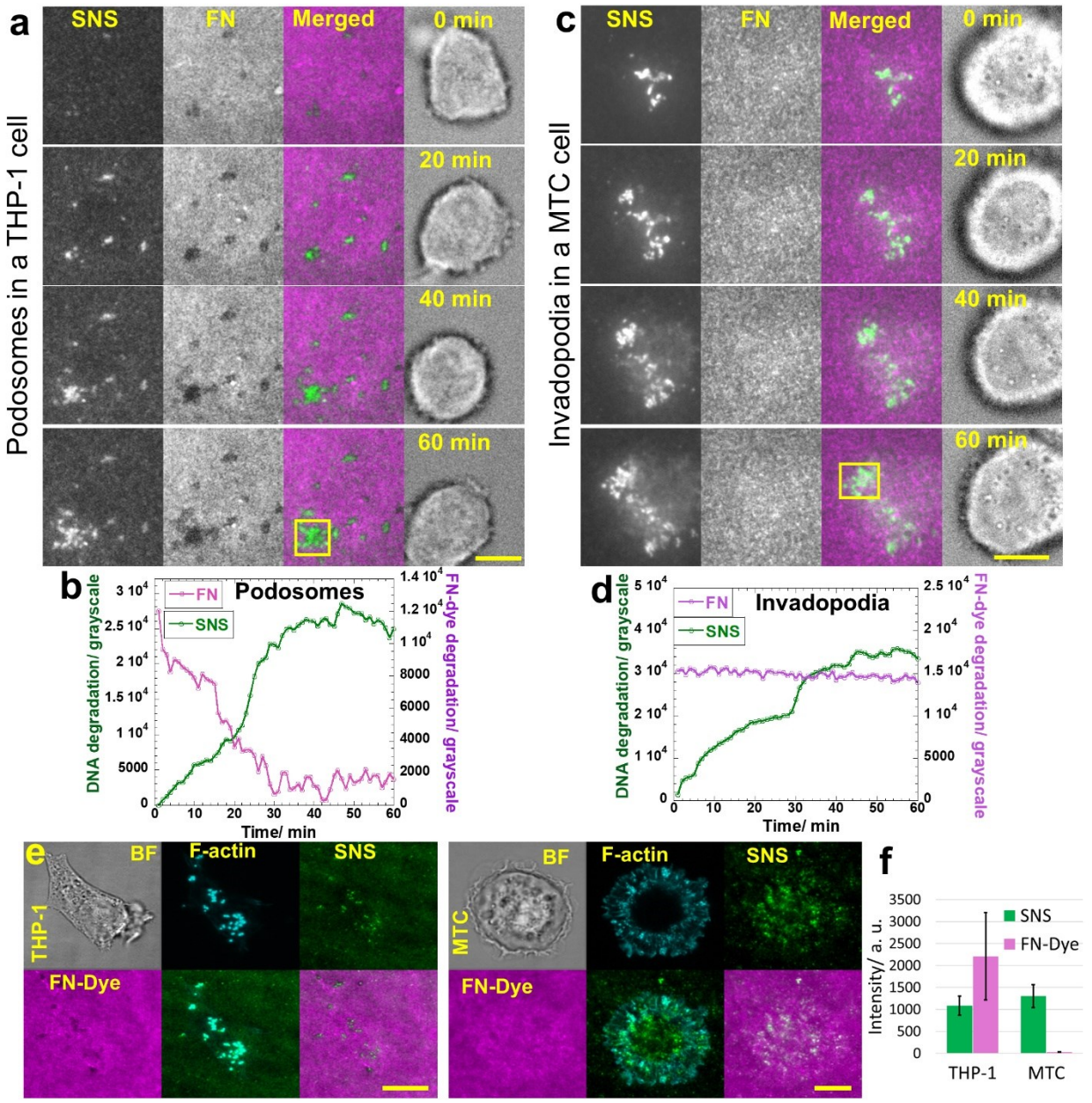

Fig. 5. Co-degradation of SNS (extracellular DNA) and HyLite488-labeled fibronectin (matrix protein) by invadosomes. (**a**) A podosome forming THP-1 cell was imaged over 60 min on a surface coated with both SNS and HyLite488-labeled FN (Video 2). (**b**) Fluorescence intensity analysis shows that the degradation of both SNS and FN is starting at a similar time by podosome. (**c**) Invadopodia forming MTC cell on a surface coated with both SNS and HyLite488-labeled FN (Video 3). (**d**) Fluorescence intensity analysis shows that only SNS was degraded by invadopodia, no degradation of FN was observed within the time frame of the experiment. (**e**) THP-1 and MTC with immunostained F-actin on surface, coated with SNS and FN-dye. (**f**) DNase activity and protease activity in invadopodia (in MTC cells) and podosomes (in THP-1 cells). The statistical analysis was based on 20 cells. Error bars represent standard deviations. Scale bar: 10 µm.

DNase-active podosome rosettes target and surround surface-immobilized *E. coli*

As invadosomes are formed in various cell types, the function of DNase in invadosomes is likely versatile. Here we studied the physiological role of DNase in macrophages which form rich podosomes. Because the main function of macrophages is to serve as an immune defense to ingest invading pathogens which potentially carry pathogenic DNA, we studied DNase activity in podosomes with the presence of pathogens and immunogenic materials. On an SNS surface, a macrophage-like cell (THP-1) formed podosomes at cell peripheral region and constantly degraded surface-immobilized DNA, probing and patrolling on the surface (Fig. 6a, Video 4). When encountering pathogens (*E. coli* immobilized on the SNS surface), podosomes and DNase immediately targeted the pathogens and started reacting around them (Fig. 6b, Video 5). Eventually podosomes formed in a rosette pattern around the immobilized *E coli* (Fig. 6c), while DNase in the podosomes degrades extracellular DNA (the SNS) in the peripheral region around the *E coli*, until the *E. coli* were engulfed by the macrophage. Co-imaging of SNS signal and F-actin stained by phalloidin confirmed that the SNS signal of THP-1 cells around the *E*. coli originated from podosomes (Fig. 6d). This assay revealed that DNase-active podosomes preferentially form around pathogens, suggesting that podosomes in macrophages may have a direct role in targeting and engaging pathogens and destroying DNA in the proximity of the pathogens.

DNase-active podosomes form around antigen islets

To further confirm that the formation of podosomes and DNase activity around pathogenic targets are specific immune responses, we tested THP-1 cells on a glass surface printed with micron-sized antigen islets (donkey IgG) and coated with SNS in the background. The whole surface was also coated with poly-L-lysine to assist THP-1 cell adhesion. The IgG is foreign substance that can elicit immune reaction of macrophages (Arend and Mannik, 1973). Co-imaging of F-actin and DNase activity showed that DNase-active podosomes are indeed preferentially formed around the antigen islets (Fig. 6e), suggesting that podosome formation and the associated DNase activity were purposed immune responses. Collectively, we demonstrated that DNase activity in podosomes targets and surrounds immunogenic sources, possibly functioning as a defense mechanism by degrading potential foreign genetic material carried by pathogens. This study shows the immunological implications of podosomes in macrophages, and suggests that DNase in podosomes could be the first-line weaponry destroying genetic material originated from pathogens.

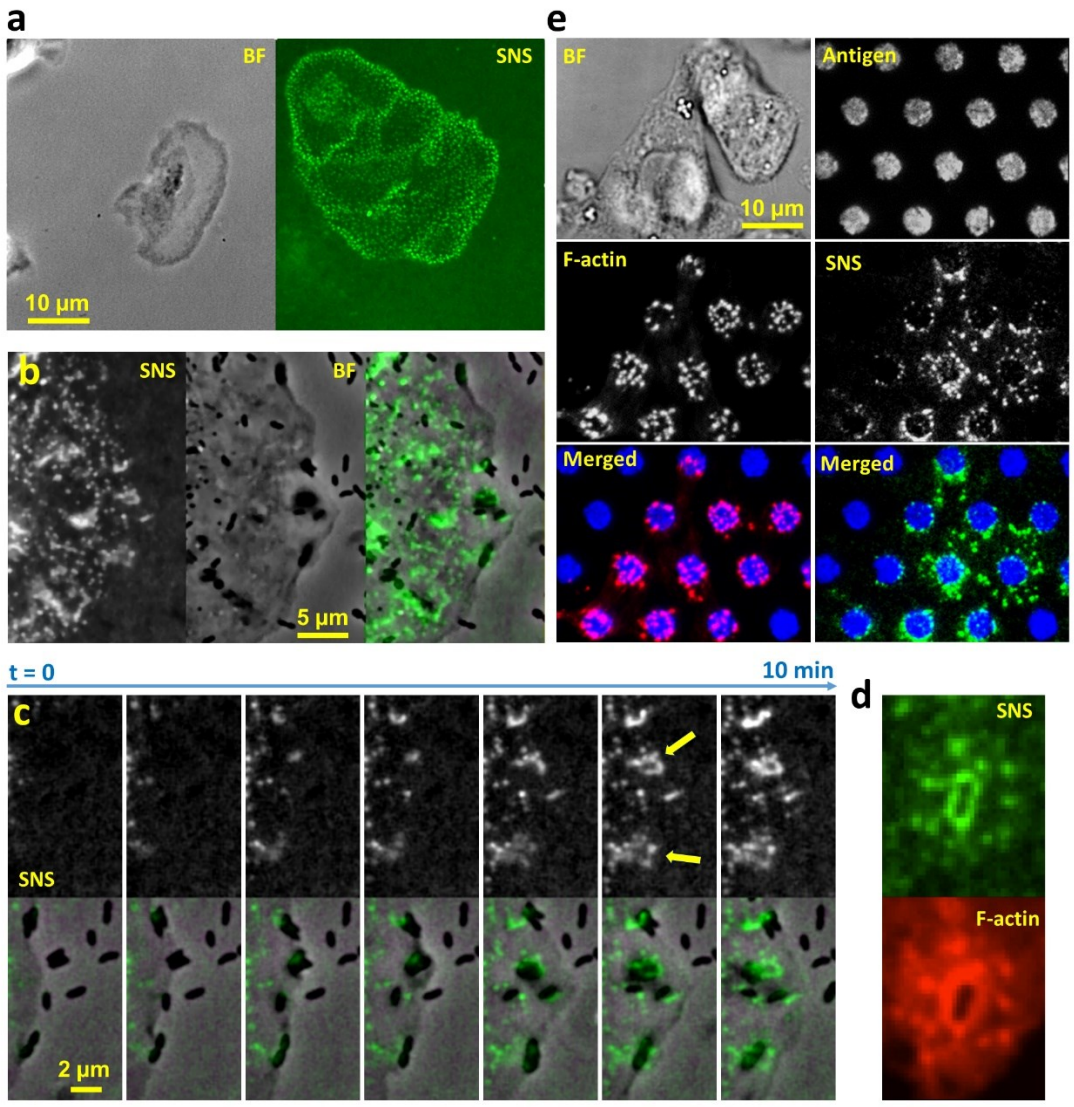

Fig. 6. DNase-active podosomes respond to pathogens and immunogenic material. (a) A migrating macrophage-like cell (THP-1) formed dense podosomes in the leading edge and degraded the surface DNA along the path (Video 4). (**b)** A macrophage-like cell (THP-1) specifically reacted to surface-immobilized *E. coli* (dark short rod-like objects) with DNase activity (Video 5). (**c**) DNase-active podosomes formed around surface-immobilized *E. coli* in a rosette pattern (yellow arrows), degrading the local extra-cellular DNA (SNS), until the *E. coli* were internalized. (**d**) Co-imaging of SNS signal and F-actin of a THP-1 cell around a bacterium. (**e**) THP-1 cells formed podosome rosettes around the antigen (donkey IgG) islands (size = 5 µm) and degraded the surrounding surface DNA, showing general reaction to the immunogenic material by forming DNase-active podosomes. Note that SNS was not coated on the IgG islands but coated in the background.

Podosomes degrade bacterial DNA extracellularly by contact

As we demonstrated that macrophages preferentially form podosomes on immunogenic materials, we further tested whether these podosomes are capable of degrading pathogenic DNA directly without the need of internalizing it. First, we extracted crude DNA from *E. coli* and immobilized

the DNA uniformly on a glass surface according to the protocol in the Materials and Methods section. THP-1 cells activated with TGF-β1 were plated on the surface. After 1 h incubation, the cells were fixed and permeabilized and Sytox green was used to stain the bacterial DNA on the surface. TIRF imaging showed that podosomes formed on the surface, and the majority of podosomes degraded the surface-immobilized DNA, suggesting that podosomes in macrophages can degrade bacterial DNA immobilized on a surface (Fig. 7a). To further demonstrate that podosomes can directly degrade chromosomal DNA released by pathogens, we immobilized *E. coli* on a surface and lysed them on site with lysozyme. Chromosomal DNA was spilled out from individual *E. coli* and immobilized locally on the surface. Activated THP-1 cells were cultured on the surface and shown to degrade bacterial chromosomal DNA on the surface (Fig. 7b, indicated by the yellow arrows). Collectively, these experiments showed that podosomes in macrophages are able to degrade pathogenic DNA extracellularly, revealing an important yet unreported role of DNase-active podosomes in immune response and extracellular DNA clean-up.

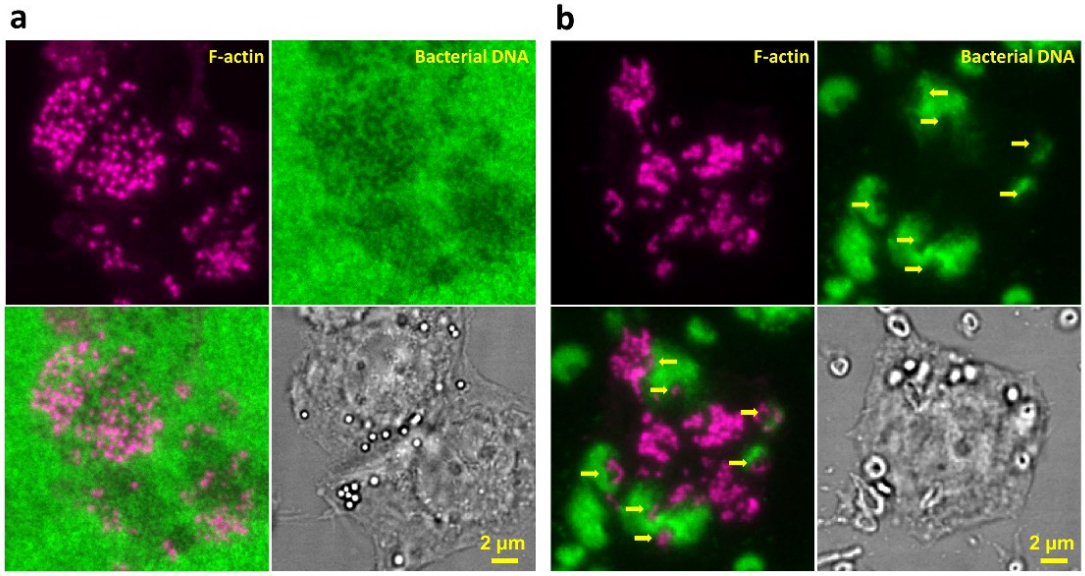

Fig. 7. DNase-active podosomes degrade bacterial DNA in an extracellular manner. (a) THP-1 cells on a surface uniformly coated with bacterial DNA extracted from *E. coli*. The DNA was stained with Sytox green. **(b)** A THP-1 cell on a surface decorated with chromosomal DNA spilled by individual *E. coli* lysed on site. The yellow arrows indicate the DNA degrading sites. The DNA was stained with Sytox green.

Discussion

In summary, we reported DNase activity in both podosomes and invadopodia, characterized its temporal dynamics, and confirmed its identity. The DNase activity in invadosomes is strong, prompt, localized, and ubiquitous in invadosomes across different cell types and species, suggesting that invadosomes generally recruit DNase. We then identified it as membrane-bound DNase X. The DNase X may work with proteases in parallel to degrade ECM, which consists of both matrix proteins and extracellular DNA released by dead cells and pathogens (Aucamp et al., 2018; Brinkmann et al., 2004). DNase activity is more consistent than protease activity in invadosomes, potentially making it a more robust bio-marker of invadosomes to set them apart from other cell-adhesion units such as focal adhesions, lamellipodia, and filopodia (Kelly et al.,

1994). The presence of DNase in invadosomes also provides new therapeutic targets and cautions for researchers in performing gene-based therapeutics to invadopodium-forming cancer cells.

The ubiquitous DNase activity in invadosomes suggests that its function is likely versatile. Here we preliminarily investigated the immunological role of DNase activity in podosomes of macrophages. Our results showed that the DNase-active podosomes preferentially form around micron-sized antigen islets and pathogens. We further showed that podosomes in macrophages are indeed capable of degrading pathogenic DNA by contact, without the need of DNA internalization. Collectively, podosome formation elicited by immunogenic sources and pathogenic DNA degradation caused by podosomal DNase, suggest that podosomal DNase plays an important role in immune surveillance, defense and extracellular DNA clean-up. Invadosomal DNase has likely more physiological functions than shown in this work, as its presence is ubiquitous in invadosomes which are formed in many cells including metastatic cancer cells and matrix-remodeling cells (osteoblasts).

Overall, revealing DNase in invadosomes adds an important piece in the whole picture of enzymatic behaviors in these dynamic and versatile structures. To the best of our knowledge, this is the first report of DNase activity in invadosomes since their discovery decades ago. The absence of DNase study in invadosomes in the past could be due to the lack of a sensor that can image the DNase activity at the cell-substrate interface. This work will likely intrigue more research to study the physiological roles of DNase in invadosomes and the associated signaling pathways, and the DNase sensor SNS would be a valuable tool to bring the DNase activity to light.

Acknowledgements

We thank Dr. Kaitlin Bratlie for sharing the RAW264.7 cell-line and Dr. Ian Schneider for sharing MTC cell-line.

Funding

This work was supported by National Science Foundation (1825724) and National Institute of General Medical Sciences (1R35GM128747).

Author contributions

XW, KP and YZ conceived the project. KP and YZ performed the experiments. KP, YZ and XW analyzed the data. XW and KP wrote the manuscript.

Competing interests

The authors declare that they have no competing interests.

Materials and Methods

Synthesis of SNS: We customized and ordered oligonucleotides from Integrated DNA Technologies (IDT) with sequences and modifications as shown below (Sequence from 5′ end to 3′ end):

DNA 1: GGG CGG CGA CCT CAG CAT/3BHQ_2/
DNA 2: /5BiosG/T/iCy3/ATG CTG AGG TCG CCG CCC/
DNA 3: GGG CGG CGA CCT CAG CAT
DNA 4: /5Cy3/ AGG TCG ATG CTG CCG CCC/3Bio/

For the construction of SNS, DNA 1 and DNA 2 dissolved in 1× phosphate buffered saline (PBS) were annealed at a molar ratio of 1.2:1.0 and stored at 4ºC at a final concentration 10 μM for further use. For the construction of Cy3-labeled DNA, DNA 3 and DNA 4 were annealed in the same conditions as SNS annealing.

SNS immobilization on the glass surface: The imaging platform for our study is the SNS-immobilized glass surface. To prepare this surface, we follow these steps. Step 1: a solution of 200 μg/mL BSA-biotin (biotin conjugated Bovine serum albumin, A8549, Sigma-Aldrich, USA) and 2 μg/mL fibronectin (1918-FN, R&D System, USA) in PBS buffer was incubated on a glass-bottom petri dish (D35-14-1.5-N, in vitro Scientific, CA, USA) for 30 min at 4ºC. BSA and fibronectin both can be physically adsorbed on the glass surface. Fibronectin was used for assisting cells in adhering. The surface was rinsed with cold PBS thrice. Step 2: The surface was then incubated with a solution of 50 μg/mL neutravidin (31000, Thermo Fisher Scientific, MA, USA) in PBS for 30 min at 4ºC and rinsed with cold PBS thrice. Step 3: The surface was then incubated with the solution of 0.1 μM SNS in PBS for 30 min at 4ºC and rinsed with PBS thrice. The glass surface became ready for cell plating and further experiments.

Fibronectin-HiLyte 488 surface preparation: A solution of 5 μg/mL Fibronectin labeled with HiLyte fluor 488 (FNR02-A, Cytoskeleton, Inc. USA) in PBS was incubated on a glass-bottom petri-dish for 30 min at 4ºC and rinsed with cold PBS thrice. The petri dish was further coated with 200 μg/mL BSA-biotin, 50 μg/mL neutravidin and 0.1 μM SNS, consecutively, and became ready for experiments.

Cell culture and cell plating: Both cancer (MDA-MB-231 and MTC) and non-cancer macrophage resembling (RAW264.7 and THP-1) cell-lines were used in SNS assays. All the cell lines were cultured according to the supplier's protocol. The macrophage activation was done with the treatment of 1 ng/mL lipopolysaccharide (L2630, Sigma Aldrich, USA) to RAW264.7 or 2 ng/mL transforming growth factor β-1(240-B/CF, R&D System, USA) to THP-1 for 24-36 hours, respectively. The RAW264.7 cells were stably transfected with LifAct-GFP. For experiments, cells were harvested at 80–90% confluency using the following method: After removing the culture medium, cells were firstly washed and incubated with cell detaching solution inside the CO_2 incubator for 5-7 min. Recipe for 1 L cell detaching solution: 100 mL 10×HBSS +10 mL 1 M HEPES + 10 mL 7.5% sodium bicarbonate + 2.4 mL 500 mM EDTA

(Ethylenediaminetetraacetic acid). The rest of the volume was made up with distilled water and PH was adjusted to 7.4. Cells were pipetted off gently from the petri dish and transferred into a 1.5 mL centrifuge tube and centrifuged for 3 min at 300g. Cell pellet was resuspended with the corresponding complete medium. The solution was then transferred on the glass surface modified with SNS and incubated for 30-60 min inside CO_2 incubator before imaging.

Fish macrophage extraction: We developed a convenient method to extract a small amount of fish macrophages from fish scales. 1-2 scales were plucked from a fantail goldfish (Carassius auratus) using a pair of flat-tip tweezers and placed on a glass bottom petri dish with the interior side of the scales contacting the glass surface. After 1-2 min, culture medium (IMDM, 30-2005, ATCC USA) spiked with 20% fetal bovine serum and 1% penicillin was added. The scales were incubated at room temperature for about 12-24 h to allow cells to migrate out. Before experiments, cells were detached from the petri dish using EDTA solution, and then harvested by centrifuging (300g for 3 min) and resuspending in culture medium. The cell solution was incubated on a SNS surface for 1 h. Maintenance of goldfish for the experiment was performed under the supervision of Institutional Animal Care and Use Committee. Log number: 8-16-8333-I.

Previously, this method was used to harvest keratocytes, a type of fast migrating cells functioning in wound healing. However, we found 10-30% cells extracted from the fish scales are actually macrophages, identified by TNF-α immunostaining, not keratocytes. These two cell types are distinctly different in terms of migration rate, podosome formation and surface DNA degradation. Keratocytes migrate at 10-20 μm/min and do not form podosomes and produce no DNA degradation signals. On SNS surfaces, macrophages can be simply identified with DNA degradation in punctate patterns.

Immunostaining: Immunostaining was started with the fixation of the cells with 4 % formaldehyde solution in PBS for 15 min at room temperature. After removing the formaldehyde solution, cells were permeabilized with 0.1% Triton X-100 solution in PBS for 20 min at room temperature. Then the cells were blocked with 5 mg/ mL BSA solution in PBS for 45 min at room temperature. For the staining of actin, Phalloidin-Alexa 405 (A30104, Thermo Fisher Scientific, USA) was used and the sample was incubated according to the supplier's instruction and washed with PBS for three times with 5 min each. For the staining of vinculin, or DNase X, cell samples were first treated with primary antibodies: anti-vinculin (90227, Millipore), anti-TKS5 (MABT336, Millipore) or anti-DNase X (H00001774-MO2, Abnova) in PBS for 1h at room temperature, and then washed with PBS for three times. PBS remained on the samples for 5 min prior to its removal. The samples were then treated with dye-labeled secondary antibody (ab175660, abcam, UK) solution in PBS and incubated for 1h at room temperature, and washed thrice with PBS with 5 min incubation time. The cortactin staining was performed with dye-labeled Anti-cortactin (05-180-AF647, Millipore).

Cell transfection: For the transfection, corresponding cells were cultured in a 35 mm petri dish up to 70-80% of confluency. Plasmid DNA (2-3 μg) was diluted in 400 μL Opti-MEM (11058021, Thermo Fisher Scientific, USA) spiked with 2-3 μL Plus reagent (15338100, Thermo Fisher Scientific, USA). The plasmid solution was mixed and incubated for 10 min at room temperature. After that, 6-8 μL Lipofectamine-LTX (15338100, Thermo Fisher Scientific, USA) was added to

the plasmid solution, which was then mixed and incubated at room temperature for 30 min. The medium in a petri dish of cells was exchanged with 2 mL fresh complete medium added with the plasmid mixture. Cells were incubated in an incubator for 18-24 h. Before experiments, cells were detached with EDTA solution and plated on the imaging platform.

Inhibitor study: GPI inhibition: THP-1 cells activated by 2 ng/mL TGF-β1 (Transforming growth factor β1) for 36-48 h were plated on the SNS imaging plate along with 2 or 5 unit/mL of PI-PLC (P8804, Sigma Aldrich, USA) in complete growth medium for 1 h and then stained with phalloidin-Alexa 405 prior to imaging. Other inhibitors: activated cells were detached from the surface with EDTA treatment and then centrifuged in a centrifuge tube. The pellet was resuspended in complete medium with desired concentrations of inhibitors: blebbistatin (B0560, Sigma Aldrich) at 10 μM and cytochalasin D (C8273, Sigma Aldrich) at 0.5 μM, respectively. The cell suspensions with inhibitors were plated on the imaging substrate and incubated in CO_2-incubator before imaging.

siRNA-mediated DNase X knockdown: THP-1 cells were harvested and resuspended in serum-free RPMI medium were plated in a 24-well plate (800 μL per well). For transfection of DNase X siRNA (sc-77165, Santa Cruz Biotechnology, USA), 2 μL of 10 μM siRNA and 2 μL Lipofectamine RNAiMAX (13778100, Thermo Fisher Scientific, USA) was added to 200 μL Opti-MEM (31985062, Thermo Fisher Scientific) and incubated for 15 min. The mixture was then added to the cell suspension. After 24 h, medium of the transfected cells and control cells were replaced with complete RPMI medium spiked with TGF-β1 at 2 ng/ mL concentration. After 48 h, these cells were plated on SNS-coated surfaces and incubated for 90 min in an incubator with 5% CO_2. F-actin immunostaining was performed for the identification and quantification of DNase activity. Cells were imaged by a TIRF microscope and results were analyzed with 20 cells from both the control group and the transfected cell group.

Immobilization of *E. coli* on SNS surfaces: The immobilization of the *E. coli* (DH10B) was performed in following steps: First, the glass bottom Petri dish was coated with 1 μg/mL PLL (poly-L-lysine, P7890, Sigma Aldrich, USA) in milli-Q water for 30 min and washed thrice with milli-Q water. The *E. coli* was harvested by three cycles of centrifuging (10,000 RCF), discarding supernatant and resuspending in milli-Q water. Bacteria solution after density adjustment was transferred onto the PLL coated Petri dish and incubated for 30 min at room temperature. Wash the *E. coli* immobilized PLL surface thrice with milli-Q water. Continue to perform SNS coating according to above described method.

IgG micro-patterning: The glass bottom petri dish was first coated with 10 μg/mL PLL in milli-Q water for 30 min and then washed with milli-Q water for three times. The surface was blown to dry with a stream of compressed air. A drop of 10 μL solution (100 μg/mL) of Donkey anti-rabbit IgG conjugated with Alexa 405 (ab175651, Abcam) was placed onto a clean glass slide and a PDMS stamp (5 μm diameter, 10 μm spacing and 5 μm pillar height for each dot, Research Micro Stamps, USA) was placed onto the droplet (facing the micro-patterned surface towards the droplet) and incubated for 10 min. The stamp was then taken off the antigen-solution droplet and residual liquid on the stamp was blown off with compressed air. The stamp was placed onto the PLL surface for 10 min and carefully retracted afterward. Note that the stamp should not have horizontal motion

relative to the PLL surface to avoid smearing the surface. The surface was washed with milli-Q water thrice and SNS coating was performed on the surface according to usual method.

THP-1 cells on bacterial DNA purified from E. coli: 50 μg/mL PLL in water was added to the well of a glass-bottom petri-dish and incubated for 20 min at room temperature. The petri-dish was washed with water three times. DNA was extracted from E. coli using high-speed plasmid mini kit (IB47101, IBI Scientific) and immobilized on the PLL-coated glass surface. The immobilization is enabled by the electrostatic force as the PLL coating is positively charged and DNA backbone is negatively charged. 350 ng/μL DNA solution in elution buffer (of the kit) was placed on the PLL-coated petri-dish and incubated for 30 min at the room temperature, and then washed with PBS for three times. THP-1 cells were plated in the petri-dish and incubated for 1 h in an incubator (5% CO_2 and 37ºC). The cells were then fixed and permeabilized with 4% formaldehyde and 0.2 % Triton X-100 solution, respectively. F-actin and extracellular DNA were stained with phalloidin-Alexa 647 and Sytox green, respectively, with 20 min staining time. Note that Sytox green should not be applied before THP-1 cell incubation, as Sytox green may block DNase-DNA interaction.

THP-1 cells on locally-immobilized DNA from individual E. coli: Freshly cultured E. coli were harvested by centrifuging (6000 RCF for 1 min) in a 1.5 mL centrifuge tube. The pellet was resuspended in water and re-centrifuged for three times. The E. coli suspended in water was then added on the PLL-coated petri-dish (detailed in previous paragraph) and incubated for 30 min at room temperature. The E. coli should be immobilized on the glass surface. The surface was washed with water for three times. Next, 0.5 mg/mL lysozyme (L6876; Sigma-Aldrich) in 25 mM Tris-HCL buffer (pH 8.0 with 50 mM glucose and 10 mM EDTA) was added in the petri-dish and incubated at 37ºC for 4 h to lyse the E. coli on-site. The surface was washed with PBS for three times. The chromosomal DNA from individual E. coli was spilled out and immobilized locally on the PLL surface. THP-1 cells were then plated on the petri-dish and incubated for 1 h in an incubator (5% CO_2 and 37ºC). Cells were fixed and permeabilized with 4% formaldehyde and 0.2 % Triton X-100 solution respectively. F-actin and extracellular DNA were stained with phalloidin-Alexa 647 and Sytox green, respectively, by incubating for 20 min at room temperature.

Microscopy and image processing: All static and time-lapse imaging was performed using total internal reflection (TIRF) microscopy setup (Nikon Ti-2) with a 100X oil immersion objective. Images and Data were analyzed by Matlab code developed in our lab.

Methods of Statistics: The main body of data in this manuscript is in the format of images and videos. Quantification of fluorescence intensities of target signals in these images and videos was performed with Matlab code compiled by ourselves. The graphs for data presentation were prepared with a software, Kaleidagraph. p values were evaluated with two-tailed test with the command “ttest” in Matlab. Data distributions were generally assumed to be normal but they were not formally tested.

Online supplemental materials: Video 1 shows real-time DNase activity and actin core nucleation on SNS surface by a lifeAct-GFP transfected RAW264.7 cell. Video 2 shows DNA and matrix protein co-degradation by a THP-1 cell. Video 3 shows DNA and matrix protein co-degradation by an MTC cell. Video 4 displays how a migrating macrophage degrade dsDNA at the cell front in punctate form and Video 5 showing how THP-1 cell reacted to surface immobilized *E. coli*. Fig. S1 shows that podosomes in THP-1 cells degraded dsDNA regardless of their sequences, but degraded neither ssDNA nor PNA/DNA hybrid. Fig. S2 shows the identification of fish macrophages using TNF-α immunostaining. Fig. S3 shows the colocalization of cortactin and F-actin in MTC and MDA-MB-231 cells. Fig. S4 shows the colocalization of TKS5 and F-actin in MDA-MB-231 cell. Fig. S5 shows DNase activity in podosome depends on actin polymerization but not depends on myosin II. Fig. S6. Shows that siRNA knockdown reduced the expression level of DNase X in THP-1 cells.

References:

Albiges-Rizo, C., O. Destaing, B. Fourcade, E. Planus, and M.R. Block. 2009. Actin machinery and mechanosensitivity in invadopodia, podosomes and focal adhesions. *J. Cell Sci.* 122:3037-3049.

Arend, W.P., and M. Mannik. 1973. The macrophage receptor for IgG: number and affinity of binding sites. *J. Immunol.* 110:1455-1463.

Artym, V.V., Y. Zhang, F.O. Seillier-Moiseiwitsch, K.M. Yamada, and S.C. Mueller. 2006. Dynamic interactions of cortactin and membrane type 1 matrix metalloproteinase at invadopodia: Defining the stages of invadopodia formation and function. *Cancer Res.* 66:3034-3043.

Aucamp, J., A.J. Bronkhorst, C.P.S. Badenhorst, and P.J. Pretorius. 2018. The diverse origins of circulating cell-free DNA in the human body: a critical re-evaluation of the literature. *Biol. Rev.* 93:1649-1683.

Badowski, C., G. Pawlak, A. Grichine, A. Chabadel, C. Oddou, P. Jurdic, M. Pfaff, C. Albiges-Rizo, and M.R. Block. 2008. Paxillin phosphorylation controls invadopodia/podosomes spatiotemporal organization. *Mol. Biol. Cell*. 19:633-645.

Berdeaux, R.L., B. Diaz, L. Kim, and G.S. Martin. 2004. Active Rho is localized to podosomes induced by oncogenic Src and is required for their assembly and function. *J. Cell Biol.* 166:317-323.

Branch, K.M., D. Hoshino, and A.M. Weaver. 2012. Adhesion rings surround invadopodia and promote maturation. *Biol. Open*. 1:711-722.

Brinkmann, V., U. Reichard, C. Goosmann, B. Fauler, Y. Uhlemann, D.S. Weiss, Y. Weinrauch, and A. Zychlinsky. 2004. Neutrophil extracellular traps kill bacteria. *Science*. 303:1532-1535.

Buccione, R., J.D. Orth, and M.A. McNiven. 2004. Foot and mouth: Podosomes, invadopodia and circular dorsal ruffles. *Nat. Rev. Mol. Cell Bio.* 5:647-657.

Chen, W.T., J.M. Chen, S.J. Parsons, and J.T. Parsons. 1985. Local Degradation of Fibronectin at Sites of Expression of the Transforming Gene-Product Pp60src. *Nature*. 316:156-158.

Cougoule, C., V. Le Cabec, R. Poincloux, T. Al Saati, J.L. Mege, G. Tabouret, C.A. Lowell, N. Laviolette-Malirat, and I. Maridonneau-Parini. 2010. Three-dimensional migration of macrophages requires Hck for podosome organization and extracellular matrix proteolysis. *Blood*. 115:1444-1452.

Dalaka, E., N.M. Kronenberg, P. Liehm, J.E. Segall, M.B. Prystowsky, and M.C. Gather. 2020. Direct measurement of vertical forces shows correlation between mechanical activity and proteolytic ability of invadopodia. *Sci. Adv.* 6.

Desai, B., T. Ma, and M.A. Chellaiah. 2008. Invadopodia and matrix degradation, a new property of prostate cancer cells during migration and invasion. *J. Biol. Chem.* 283:13856-13866.

Eddy, R.J., M.D. Weidmann, V.P. Sharma, and J.S. Condeelis. 2017. Tumor Cell Invadopodia: Invasive Protrusions that Orchestrate Metastasis. *Trends Cell Biol.* 27:595-607.

Jacob, A., and R. Prekeris. 2015. The regulation of MMP targeting to invadopodia during cancer metastasis. *Front. Cell Dev. Biol.* 3:4.

Kelly, T., S.C. Mueller, Y.Y. Yeh, and W.T. Chen. 1994. Invadopodia Promote Proteolysis of a Wide Variety of Extracellular-Matrix Proteins. *J. Cell Physiol.* 158:299-308.

Linder, S., D. Nelson, M. Weiss, and M. Aepfelbacher. 1999. Wiskott-Aldrich syndrome protein regulates podosomes in primary human macrophages. *Proc. Natl. Acad. Sci. USA*. 96:9648-9653.

Linder, S., C. Wiesner, and M. Himmel. 2011. Degrading Devices: Invadosomes in Proteolytic Cell Invasion. *Annu. Rev. Cell Dev. Biol.* 27:185-211.

Lochter, A., M.D. Sternlicht, Z. Werb, and M.J. Bissell. 1998. The significance of matrix metalloproteinases during early stages of tumor progression. *Ann. N.Y. Acad. Sci.* 857:180-193.

Mueller, S.C., Y.Y. Yeh, and W.T. Chen. 1992. Tyrosine Phosphorylation of Membrane-Proteins Mediates Cellular Invasion by Transformed-Cells. *J. Cell Biol.* 119:1309-1325.

Murphy, D.A., and S.A. Courtneidge. 2011. The 'ins' and 'outs' of podosomes and invadopodia: characteristics, formation and function. *Nat. Rev. Mol. Cell Bio.* 12:413-426.
Parrish, J.E., A. Ciccodicola, M. Wehnert, G.F. Cox, E. Chen, and D.L. Nelson. 1995. A Muscle-Specific Dnase I-Like Gene in Human Xq28. *Hum. Mol. Genet.* 4:1557-1564.
Paulick, M.G., and C.R. Bertozzi. 2008. The glycosylphosphatidylinositol anchor: a complex membrane-anchoring structure for proteins. *Biochemistry*. 47:6991-7000.
Paz, H., N. Pathak, and J. Yang. 2014. Invading one step at a time: the role of invadopodia in tumor metastasis. *Oncogene*. 33:4193-4202.
Poincloux, R., F. Lizarraga, and P. Chavrier. 2009. Matrix invasion by tumour cells: a focus on MT1-MMP trafficking to invadopodia. *J. Cell Sci.* 122:3015-3024.
Poulter, N.S., A.Y. Pollitt, A. Davies, D. Malinova, G.B. Nash, M.J. Hannon, Z. Pikramenou, J.Z. Rappoport, J.H. Hartwig, D.M. Owen, A.J. Thrasher, S.P. Watson, and S.G. Thomas. 2015. Platelet actin nodules are podosome-like structures dependent on Wiskott-Aldrich syndrome protein and ARP2/3 complex. *Nat. Commun.* 6.
Rafiq, N.B.M., Y. Nishimura, S.V. Plotnikov, V. Thiagarajan, Z. Zhang, S. Shi, M. Natarajan, V. Viasnoff, P. Kanchanawong, G.E. Jones, and A.D. Bershadsky. 2019. A mechano-signalling network linking microtubules, myosin IIA filaments and integrin-based adhesions. *Nat. Mater.* 18:638-649.
Raynaud-Messina, B., L. Bracq, M. Dupont, S. Souriant, S.M. Usmani, A. Proag, K. Pingris, V. Soldan, C. Thibault, F. Capilla, T. Al Saati, I. Gennero, P. Jurdic, P. Jolicoeur, J.L. Davignon, T.R. Mempel, S. Benichou, I. Maridonneau-Parini, and C. Verollet. 2018. Bone degradation machinery of osteoclasts: An HIV-1 target that contributes to bone loss. *Proc. Natl. Acad. Sci USA*. 115:E2556-E2565.
Ridley, A.J. 2011. Life at the Leading Edge. *Cell*. 145:1012-1022.
Saltel, F., T. Daubon, A. Juin, I.E. Ganuza, V. Veillat, and E. Genot. 2011. Invadosomes: Intriguing structures with promise. *Eur. J. Cell Biol.* 90:100-107.
Shiokawa, D., T. Matsushita, Y. Shika, M. Shimizu, M. Maeda, and S.I. Tanuma. 2007. DNase X is a glycosylphosphatidylinositol-anchored membrane enzyme that provides a barrier to endocytosis-mediated transfer of a foreign gene. *J. Biol. Chem.* 282:17132-17140.
Tarone, G., D. Cirillo, F.G. Giancotti, P.M. Comoglio, and P.C. Marchisio. 1985. Rous-Sarcoma Virus-Transformed Fibroblasts Adhere Primarily at Discrete Protrusions of the Ventral Membrane Called Podosomes. *Exp. Cell Res.* 159:141-157.
Uekita, T., Y. Itoh, I. Yana, H. Ohno, and M. Seiki. 2001. Cytoplasmic tail-dependent internalization of membrane-type 1 matrix metalloproteinase is important for its invasion-promoting activity. *J Cell Biol*. 155:1345-1356.
Van Goethem, E., R. Guiet, S. Balor, G.M. Charriere, R. Poincloux, A. Labrousse, I. Maridonneau-Parini, and V. Le Cabec. 2011. Macrophage podosomes go 3D. *Eur. J. Cell Biol.* 90:224-236.
Wagenaar-Miller, R.A., L. Gorden, and L.M. Matrisian. 2004. Matrix metalloproteinases in colorectal cancer: Is it worth talking about? *Cancer Metast. Rev.* 23:119-135.
Wang, Y., Y. Zhao, A. Sarkar, and X. Wang. 2019. Optical sensor revealed abnormal nuclease spatial activity on cancer cell membrane. *J Biophotonics*. 12:e201800351.
Winer, A., S. Adams, and P. Mignatti. 2018. Matrix Metalloproteinase Inhibitors in Cancer Therapy: Turning Past Failures Into Future Successes. *Mol. Cancer Ther.* 17:1147-1155.